Lyapunov exponent, stretching numbers, and islands of stability of the kicked top

V. Constantoudis and N. Theodorakopoulos
Theoretical and Physical Chemistry Institute, National Hellenic Research Foundation, Vasileos Constantinou 48, GR-11635 Athens, Greece

(Received 6 February 1997)

The Lyapunov exponent of the kicked top is evaluated as a function of the anisotropy parameter for a special value of the magnetic field ($\pi/2$). A series of ''wiggles'' is found, which coincides with the stabilization of the (Larmor) 4-cycle. The presence of islands of stability around of the 4-cycle is associated with distinct deformations of the unstable manifold and a concomitant proliferation of negative stretching numbers; the latter are thought to be responsible for the anomalous Lyapunov behavior. [S1063-651X(97)02611-1]

PACS number(s): 05.45.+b, 75.10.Hk, 67.57.Lm

I. INTRODUCTION

Any concise yet reasonably complete description of chaos in a dynamical system should, at least in principle, attempt to distinguish between the extent and intensity of chaos, i.e, account separately for the prevalence of chaotic over nonchaotic behavior, and the degree of the instability that characterizes chaotic behavior. Practical attempts to quantify chaos rely by necessity on global measures of chaotic behavior, such as the Kolmogorov entropy or, at best, individual Lyapunov exponents (LEs). Such measures are generically incomplete in an ''order-within-chaos'' situation: Whereas a long-time probe of nonlinear dynamics will in general respond to the existence of some atypical feature in an otherwise chaotic regime, it cannot *a priori* be used to identify its nature (e.g., island of stability and sticky orbit). Local measures of chaos on the other hand, are potentially very powerful tools, probing dynamical behavior in phase space and allowing for a detailed analysis of atypical behavior.

The kicked top offers a unique opportunity to explore the complementary nature of global vs local measures of chaos. At a special value of the magnetic field ($B=\pi/2$) the competing dynamics of Larmor precession (period 4) around the x axis vs free rotation around the z axis (dictated by the anisotropy) give rise to an order-within-chaos scenario; islands of stability for a ''Larmor'' 4-cycle develop for such values where the anisotropy parameter is ''in tune'' with the magnetic field. The global probe (Lyapunov exponent) is found to react to the existence of such islands, via small ''wiggles.'' In order to investigate the nature of the relationship between islands of stability and anomalies in chaotic behavior, we have made use of local probes [stretching numbers (SNs) and their spectra (SSNs) [1]]. Our findings suggest that it is possible to identify distinct areas of the unstable manifold that exhibit negative stretching numbers, i.e., locally nonchaotic behavior; these areas typically surround an island of stability and underlie the appearance of the wiggles.

This paper is organized as follows. Section II presents the model and the calculation (numerical and theoretical) of the LE. Section III deals with the spectra of stretching numbers and their relationship to the islands of stability, whereas Sec. IV discusses the relationship of the spatial distribution of (negative) SNs to the structure of the unstable manifold. Section V presents a brief discussion of our findings, along with some remarks on the feasibility of using the negative part of the SSNs as a general diagnostic tool for order-within-chaos situations.

II. LYAPUNOV EXPONENT AND ISLANDS OF STABILITY

The Hamiltonian of the classical kicked top is given by

$$H=AJ_z^2+BJ_x\sum_n \delta(t-n), \tag{2.1}$$

where A is the anisotropy and B the magnetic field, acting in bursts separated by one time unit. The dynamics of the unit angular momentum vector $\vec{J}$, determined by

$$\frac{d\vec{J}}{dt}=-\vec{J}\times\frac{\partial H}{\partial \vec{J}}, \tag{2.2}$$

leads to the discrete map

$$J_{n+1}^x=J_n^x\cos(AJ_{n+1}^z)-J_n^y\sin(AJ_{n+1}^z)\cos B + J_n^z\sin(AJ_{n+1}^z)\sin B, \tag{2.3}$$

$$J_{n+1}^y=J_n^x\sin(AJ_{n+1}^z)+J_n^y\cos(AJ_{n+1}^z)\cos B - J_n^z\cos(AJ_{n+1}^z)\sin B, \tag{2.4}$$

$$J_{n+1}^z=J_n^y\sin B+J_n^z\cos B, \tag{2.5}$$

where $\vec{J}_n$ is the spin vector immediately prior to the nth kick. The symmetries and periodic orbits of the map (2.3)–(2.5) have been studied extensively [2,3]. In this section we will compute, numerically and analytically, the (maximum) LE and study its dependence on the presence of islands of stability.

The tangent map corresponding to Eqs. (2.3)–(2.5) is given by

$$\delta\vec{J}_{n+1}=M(\vec{J}_n)\,\delta\vec{J}_n, \tag{2.6}$$

where

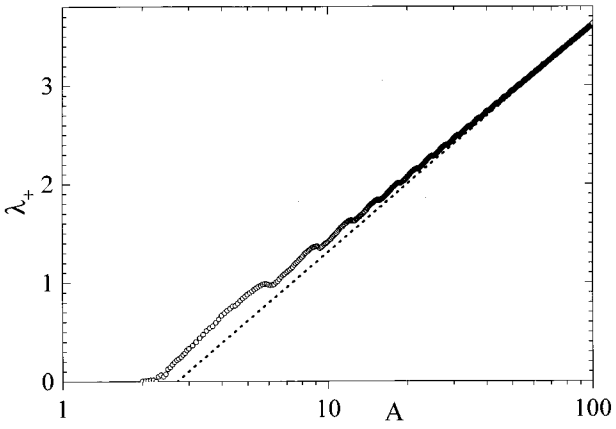

FIG. 1. (Maximum) Lyapunov exponent as a function of the anisotropy parameter for the kicked top. ($B=\pi/2$ has been used throughout the paper). The dotted line is the high-A approximation described in the text.

$$M(\vec{J}_n)=\left(\frac{\partial \vec{J}_{n+1}}{\partial \vec{J}_n}\right). \tag{2.7}$$

The largest positive LE (which in our system is equal to the Kolmogorov entropy) is given by

$$\lambda_+(A,B)=\ln\left[\lim_{N\to\infty}|j_+(N)|^{1/N}\right], \tag{2.8}$$

where $j_+(N)$ is the largest eigenvalue of the matrix product $\Pi_{n=1}^{N}M(\vec{J}_n)$. In practice we have used $N\sim 10^6$ and obtained the LEs with an accuracy of 10^{-3}, using standard procedures (cf. [4]). We are interested in the fully chaotic regime, for $B=\pi/2$ and $A\gg 1$. Chaotic regions are characterized by a single LE. The dependence of λ_+ on A is shown in Fig. 1. The result can be compared with a rough analytical estimate, which is obtained as follows (cf. the analogous arguments by Chirikov [5] on the kicked rotator).

For orbits that are strongly chaotic, it turns out that

$$\tilde{\lambda}_+(A,B)=\lim_{N\to\infty}\frac{1}{N}\sum_{n=1}^{N}\ln|\mu_+(\vec{J}_n)|, \tag{2.9}$$

where μ_+ is the largest eigenvalue of Eq. (2.7), is a reasonable approximation to Eq. (2.8). On the basis of the ergodic hypothesis, we may further substitute the time average in Eq. (2.9) with the ensemble average over the whole sphere,

$$\tilde{\lambda}_+^{\rm th}(A,B)=\frac{1}{4\pi}\int_{-1}^{1}dp\int_0^{2\pi}d\phi\,\ln|\mu_+(p,\phi;A,B)|, \tag{2.10}$$

where $p=J_z/J$ and $\phi=\arctan(J_y/J_x)$ are the canonical coordinates of our system. Finally, we make use of the approximation

$$\mu_+(p,\phi;A,B)\sim A\sqrt{1-p^2}\cos\phi\sin B, \tag{2.11}$$

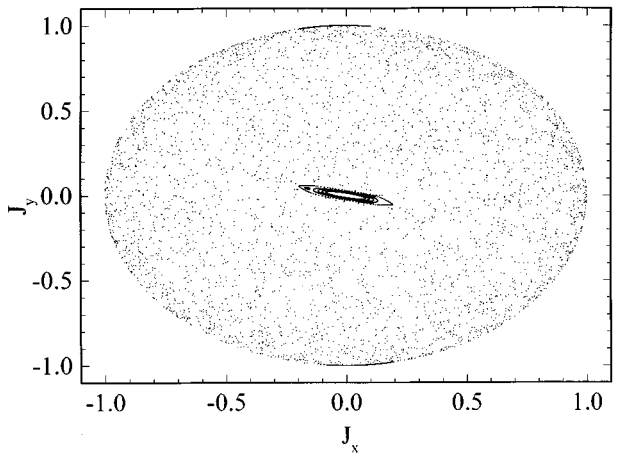

FIG. 2. Stroboscopic plot of a typical chaotic trajectory ($A=6.05$); also shown are trajectories that correspond to an island of stability around a 4-cycle.

which is valid for large A and any finite B and follows in a straightforward fashion from the (tangent) map in polar form. Introducing the approximation (2.11) in Eq. (2.10), we obtain

$$\tilde{\lambda}_+^{\rm th}(A,B)\sim\ln(A\sin B)-1, \tag{2.12}$$

displayed as a straight line in Fig. 1. What the approximation (2.12) [or its ''parent'' versions (2.10) and (2.11)] cannot deliver are the slight undulations (wiggles) of the time-averaged curve (2.8). These can be investigated by considering the stability of the periodic orbits of the mapping (2.3)–(2.5). The crucial orbit (for $B=\pi/2$, which will be assumed in the rest of the paper) is a 4-cycle consisting of the points

$$\vec{J}_1^{(4)}=\begin{pmatrix}0\\0\\1\end{pmatrix},\quad \vec{J}_2^{(4)}=\begin{pmatrix}0\\-1\\0\end{pmatrix},\quad \vec{J}_3^{(4)}=\begin{pmatrix}0\\0\\-1\end{pmatrix},\quad \vec{J}_4^{(4)}=\begin{pmatrix}0\\1\\0\end{pmatrix} \tag{2.13}$$

(for all A). The 4-cycle is stable if

$$(2\cos A+A\sin A)^2-4<0. \tag{2.14}$$

Figure 2 exhibits the island of stability around $\vec{J}_1^{(4)}$; Fig. 3 shows the first few wiggles in some more detail, along with the regions of stability of the 4-cycle, as defined by Eq. (2.14). It can be seen that the regions of stability of the 4-cycle coincide with position of dips in the LE; thus the stabilization of a particular periodic orbit appears to be responsible for the decrease in the strength of the instability (i.e., the LE) of the typical chaotic trajectory. The kicked top thus offers a unique opportunity to investigate an order-within-chaos scenario. In the next section, the more quantitative aspects of the phenomena related to the appearance of stability islands will be examined with the help of the spectrum of stretching numbers [1].

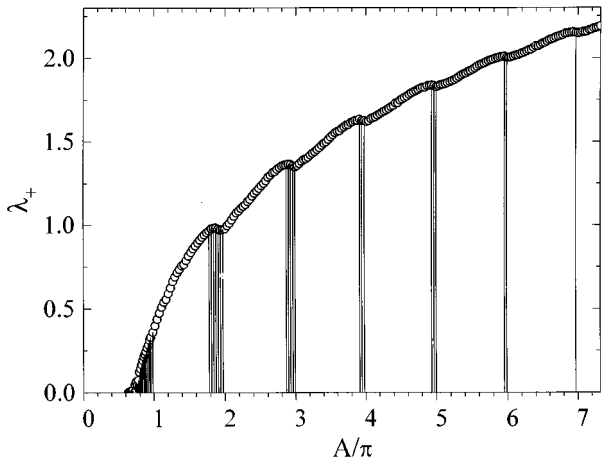

FIG. 3. Lyapunov exponent and stability regions of the 4-cycle.

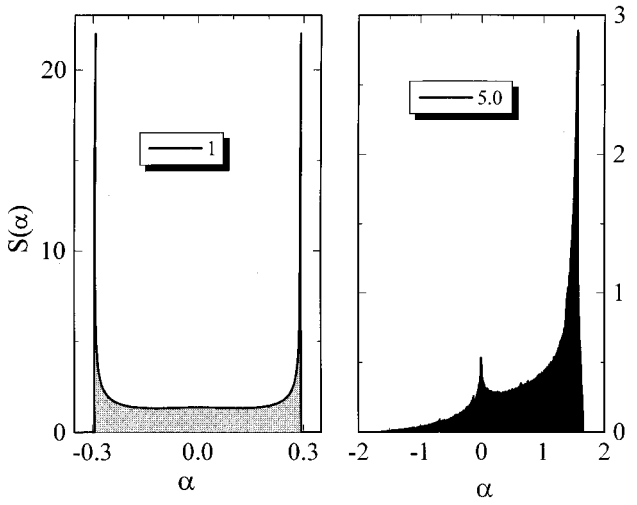

FIG. 4. Spectrum of stretching numbers for a typical regular (left) and chaotic (right) orbit. The corresponding values of the anisotropy are shown in the boxes.

III. SPECTRUM OF STRETCHING NUMBERS AND ISLANDS OF STABILITY

Lyapunov exponents, due to their emphasis on the infinite-time behavior, overlook useful dynamical information on the varying time scales and the distinct regions of phase space. For this reason, various groups [1,6–13] have studied local Lyapunov exponents and their spectra. In the case of mappings, local Lyapunov exponents, defined as the deviation of two neighboring orbits in a single iteration, are also known as stretching numbers, whereas the spectrum produced as an orbit evolves is known as the spectrum of stretching numbers [1]. An important property of the SSNs is that the spectrum produced by a single orbit is invariant, i.e., independent of the orbit's starting point; furthermore, it has been shown [1] that orbits belonging to the same chaotic region have the same SSNs, as is the case with the LEs.

In terms of the tangent map [Eq. (2.6)], the stretching number is given as

$$a_{n+1}=\ln\left\{\frac{|\delta\vec{J}_{n+1}|}{|\delta\vec{J}_n|}\right\} \tag{3.1}$$

$$=\frac{1}{2}\ln\left\{1+\frac{A^2[1-(J_n^y)^2](\delta J_n^y)^2+2A[J_n^z\delta J_n^x-J_n^x\delta J_n^z]\delta J_n^y}{|\delta\vec{J}_n|^2}\right\}, \tag{3.2}$$

where in Eq. (3.2) we have made use of $B=\pi/2$. It should be noted that in practice one rescales the norm of the vector $\delta\vec{J}_n$ after each iteration to the original value $\|\delta\vec{J}_n\|$. Since the map and the tangent map conserve the product $\vec{J}_n\cdot\delta\vec{J}_n$, the rescaling has the effect that, even if we start with a $\delta\vec{J}_0$ that has a component perpendicular to the sphere, this component will disappear after a few iterations.

The sequence of SNs $\{a_n\}$, $n=1,\ldots,N$, of length N can be characterized by its spectrum. If $\delta N(\alpha)$ is the number of SNs whose values lie in the interval $(\alpha,\alpha+\delta\alpha)$, the SSNs is defined as

$$S(\alpha)=\lim_{N\to\infty}\left(\frac{\delta N(\alpha)}{N\delta\alpha}\right). \tag{3.3}$$

The LE is the first moment of the SSNs, $\lambda_+=\int d\alpha\ \alpha\ S(\alpha)$. Typical spectra for regular and chaotic orbits are shown in Fig. 4. The numerical computations were performed with $N=10^6$ and $\delta\alpha=0.001$. Computations with different N and/or $\delta\alpha$ produced the same spectra, provided N is sufficiently large ($\geqslant 10^5$) and $\delta\alpha$ sufficiently small ($\leqslant 0.01$). It should be noted that the chaotic orbit used to generate the right spectrum of Fig. 4 ($A=5$) occupied essentially all phase space, i.e., the islands of stability are not visible. The generic feature of SSNs obtained from chaotic orbits is the monotonically increasing trend as the value of α increases; there is no large peak at negative values of α and of course no reflection symmetry (which would produce a zero first moment). Nonetheless, it will be seen that not all chaotic SSNs are entirely structureless in their left (negative α) portion; islands of stability do leave a detectable mark. In order to see this more clearly, we first present a detailed profile of

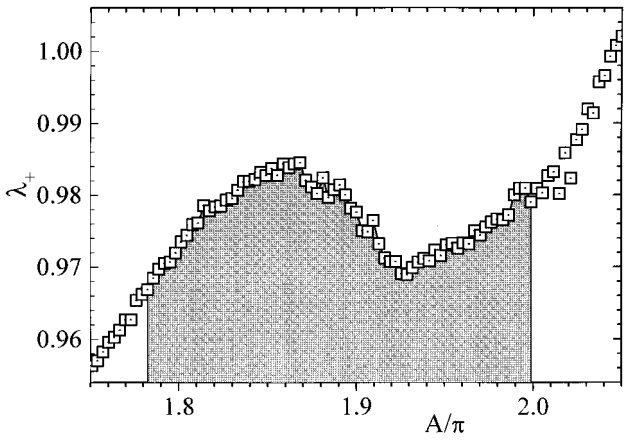

FIG. 5. Deviation of the LE vs anisotropy in the vicinity of the stability region (shaded) of a 4-cycle [as defined by Eq. (2.14)].

a wiggle; Fig. 5 exhibits the dependence of the Lyapunov exponent on the anisotropy near $A/\pi=2$. In order to obtain a higher accuracy, this calculation has been performed with $N=5\times10^6$ iterations. The decrease of λ_+ sets on at $A=5.85$ and a local minimum appears at $A=6.05$. We have obtained the SSNs for values of the anisotropy parameter close to 2π. The results are shown in Fig. 6. Because the scale is so different for positive and negative values of α, we have plotted the salient features in the negative and positive axes separately. The point to note is that the local minimum of λ_+ corresponds to the distinct peak in the negative region of the SSNs (and a concomitant dip in the positive region). In other words, even chaotic orbits may exhibit (weakly) ''structured'' SSNs on the negative side if the parameters allow some regular motion. The presence of islands of stability is thus reflected in chaotic orbits in a dual fashion: (i) in the

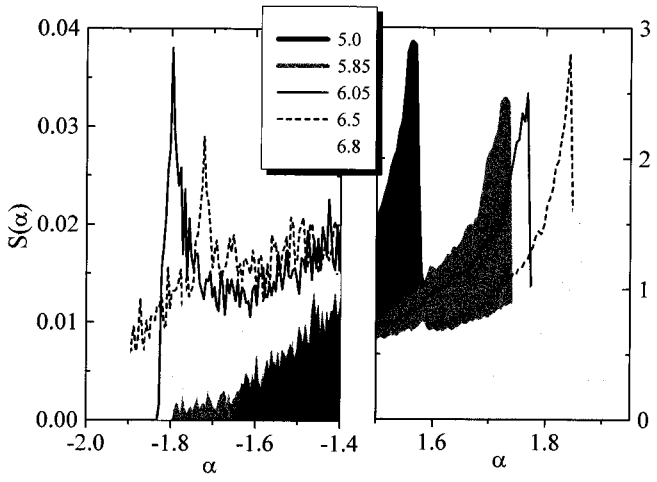

FIG. 6. Spectrum of stretching numbers for a number of values near the stability region of the 4-cycle. Note that the x axis has been split in order to emphasize details of positive SNs [right portion, where most of the contribution to the LE (first moment) originates] vs negative SNs (left portion, where the traces of nonchaotic behavior are more explicit; note, however, the difference of two orders of magnitude in the y scale). The area curves belong, respectively, to $A=5.0$ (black), 5.85 (gray), and 5.0 (light gray).

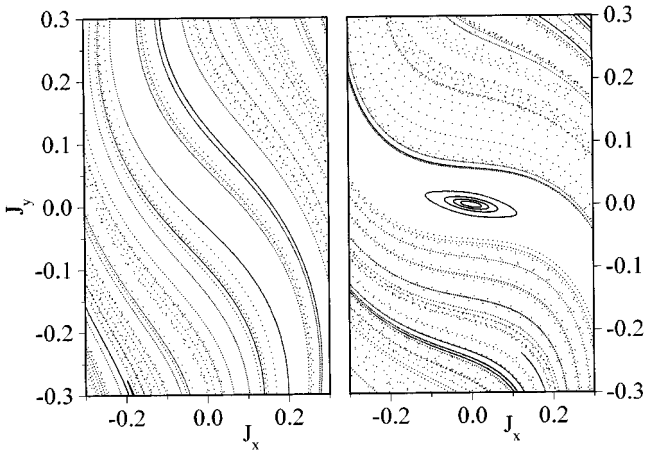

FIG. 7. Structure of the unstable manifold prior to (left, $A=5.5$) and after ($A=6.05$) the stabilization of the 4-cycle. Also shown in the right portion are typical regular trajectories around the 4-cycle.

overall measure of chaos, the Lyapunov exponent, and (ii) in an observable anomaly in the negative part of the SSNs.

IV. STRETCHING NUMBERS AND THE STRUCTURE OF THE UNSTABLE MANIFOLD

In this section we wish to pursue the relationship between islands of stability and negative SSNs anomalies by examining the structural characteristics of the latter. It is well known that whatever the direction of the initial separation $\delta\vec{J}_0$ of two neighboring chaotic orbits, after a few iterations it becomes virtually identical to the direction of the unstable manifold of the unstable fixed point. It follows from Eq. (3.2) that the value of α at the point that the orbit reaches on the nth iteration depends on the position of the point in phase space and on the direction of the difference vector $\delta\vec{J}_n$ in tangent space, which after a few iterations coincides with the direction of the unstable manifold of the map's unstable fixed points ($J_x=\pm1$, $J_y=J_z=0$) at that point. As the value of A varies, the spectrum $S(\alpha)$ changes in response to the changes that occur in the unstable manifold. This picture is supported by Fig. 7, which illustrates the structure of the unstable manifold prior to the appearance of stability islands ($A=5.5$, Fig. 7, left) and shortly thereafter ($A=6.05$, Fig. 7, right). The appearance of stability islands around the point of periodic orbit results in an unstable manifold, which, above and below the stability island, is essentially parallel to the J_y axis. This allows the second term in the second set of large curly brackets of Eq. (3.2) to dominate and favors, locally, the buildup of negative stretching numbers. The sudden appearance of such regions results in the steep rise of negative SSNs peaks against the exponentially vanishing background (cf. Fig. 6, left).

It is interesting to observe this in some detail, by following the topography of stretching numbers. In Fig. 8, right, we have plotted the points of a chaotic orbit (for $A=6.05$, i.e., at the local minimum of the Lyapunov exponent) that correspond to stretching numbers $\alpha<-1.775$. In other words, we have identified the phase-space origin of the points that con-

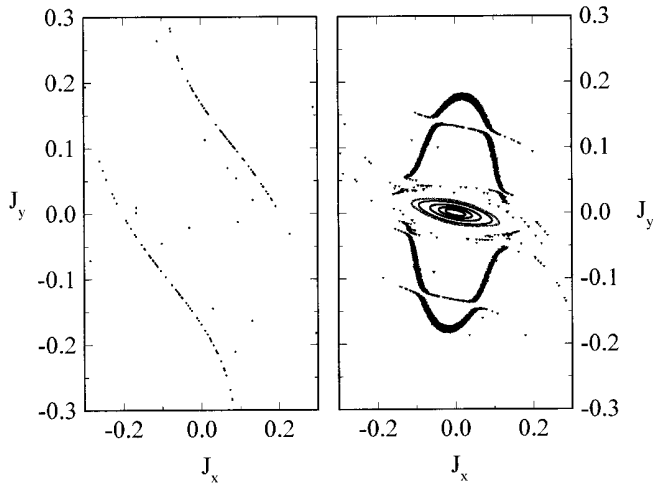

FIG. 8. Topography of the SSNs. The anisotropy parameter is as in Fig. 7. Shown at the right are all points of a given trajectory that are characterized by SNs lower than -1.775; also shown is the stability region of the 4-cycle. At the left (where the 4-cycle is still unstable), all points of a given trajectory with negative SNs are shown.

tribute to the negative SSNs peak. This should be compared with Fig. 8, left, which contains all points of a chaotic orbit with negative stretching numbers, obtained for $A=5.5$ (i.e., before the appearance of the stability island).

It should be noted that the regions of phase space that give rise to the negative SSNs (the ''Napoleon hats'' in Fig. 8, right, above and below the stability island), are relatively far from the stability islands; the chaotic orbit has no difficulty in passing through them, i.e., there is no complex structure in them, e.g., cantori or other stability islands, which might cause sticking effects and a delay of the orbit.

V. DISCUSSION AND CONCLUDING REMARKS

We have presented a model situation of an order-within-chaos scenario for the kicked top and analyzed the underlying nonlinear dynamics in terms of the anomalies in the Lyapunov exponent and the spectrum of negative stretching numbers. The detailed topography of the spectrum reveals a direct connection between the occurrence of islands of stability corresponding to periodic orbits, deformations in the structure of the unstable manifold of the parent unstable fixed point, and the local proliferation of negative stretching numbers.

Our results suggest that the presence of ordered regions (stability islands) within an otherwise chaotic environment has a direct influence on the attributes of chaotic behavior. It is perhaps instructive to follow this link by attempting to use the features of the negative SSNs as a diagnostic tool, in order to distinguish ''soft'' from ''hard'' chaos.

In order to demonstrate the feasibility of such an approach, we show Poincaré plots (Fig. 9) for typical chaotic trajectories corresponding to different values of the anisotropy parameter ($A=2.5$, 2.8, 3.5, and 5) and examine the negative portion of the SSNs obtained from the same orbits (Fig. 10). The distinct feature present in the SSNs for $A=2.5$ reflects the existence of large regions of regular motion apparent in the Poincaré plot. As the value of the anisotropy increases, the feature becomes progressively less pro-

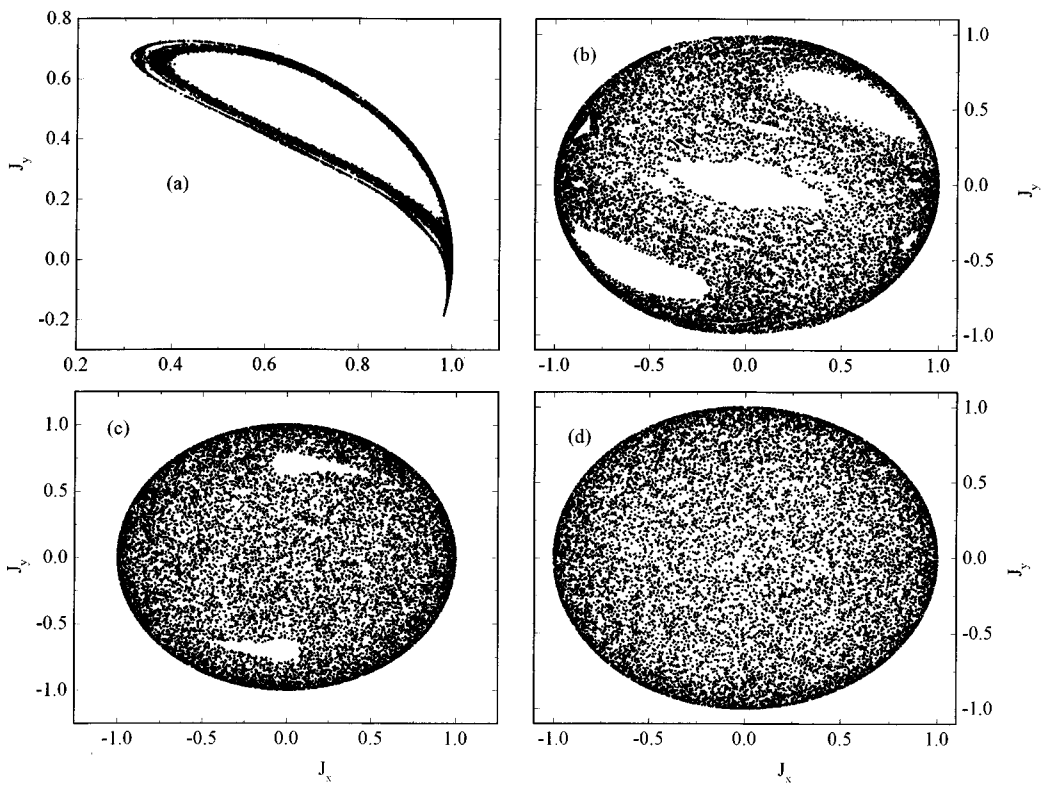

FIG. 9. Stroboscopic plots for various values of the anisotropy parameter: (a) $A=2.5$, (b) $A=2.8$, (c) $A=4.0$, and (d) $A=5.0$.

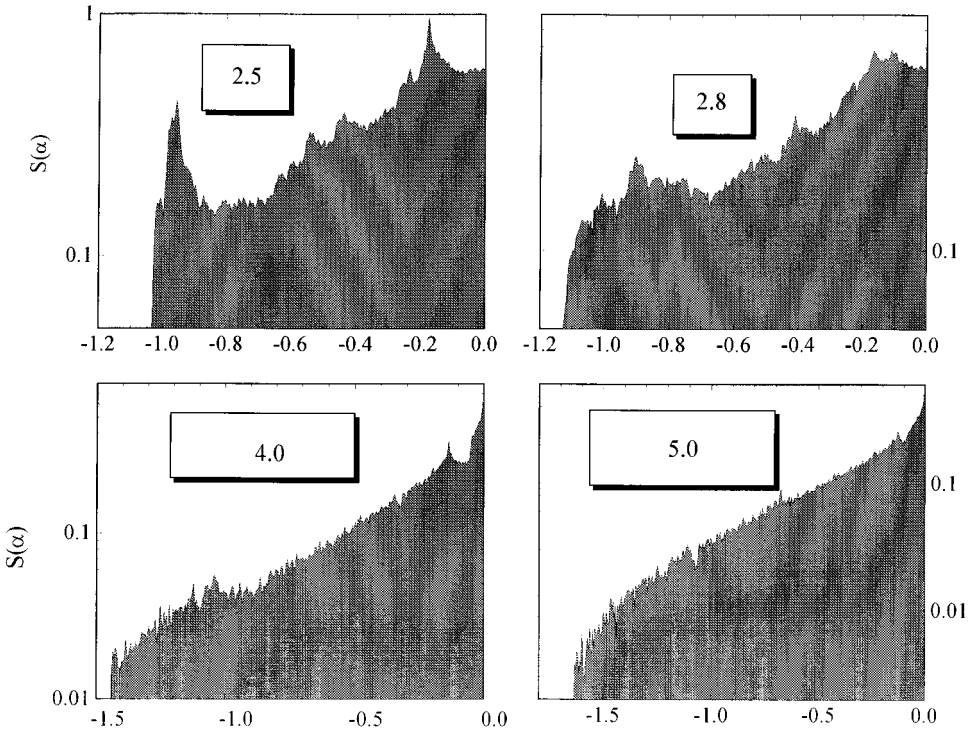

FIG. 10. SSNs for the same trajectories as in Fig. 9; the distinct feature present in the upper left portion reflects the existence of large regions of regular motion apparent in the Poincaré plot. As the value of the anisotropy increases, the feature becomes progressively less pronounced; at $A=5$, as the stroboscopic plot shows fully developed chaos, all structure has disappeared from the spectrum of negative SSNs.

nounced; at $A=5$, as the stroboscopic plot shows fully developed chaos, there is no structure whatsoever in the spectrum of negative SSNs.

The possibility of exploring order-within-chaos scenarios by looking at the spectrum of negative stretching numbers is an intriguing one. Clearly, this would only be of practical interest if successfully generalized to systems with more degrees of freedom.

[1] N. Voglis and G. J. Contopoulos, J. Phys. A **27**, 4899 (1994).
[2] F. Haake, M. Kuś, and R. Scharf, Z. Phys. B **65**, 381 (1987).
[3] G. M. D'Ariano, L. A. Evangelista, and M. Saraceno, Phys. Rev. A **45**, 3646 (1992).
[4] G. Benettin, L. Galgani, and J.-M. Strelcyn, Phys. Rev. A **14**, 2338 (1976); G. Benettin, L. Galgani, A. Giorgilli, and J.-M. Strelcyn, Meccanica **15**, 9 (1980); A. Wolf, J. B. Swift, H. L. Swinney, and J. A. Vastano, Physica D **16**, 285 (1985).
[5] B. Chiricov, Phys. Rep. **52**, 263 (1972).
[6] B. Eckhardt and D. Yao, Physica D **65**, 100 (1993).
[7] C. Amitrano and R. S. Berry, Phys. Rev. E **47**, 3158 (1993).
[8] P. Grassberger, R. Badii, and A. Politi, J. Stat. Phys. **51**, 135 (1988).
[9] H. Fujisaka, Prog. Theor. Phys. **70**, 1264 (1983)
[10] G. Haubs and H. Haken, Z. Phys. B **59**, 459 (1985).
[11] M. A. Sepulveda, R. Badii, and E. Pollak, Phys. Rev. Lett. **63**, 1226 (1989).
[12] D. J. Wales and R. S. Berry, J. Phys. B **24**, L351 (1991).
[13] H. D. I. Abarbanel, R. Brown, and M. B. Kennel, J. Nonlinear Sci. **1**, 175 (1991).